An Analysis Of Likely Scalants In The Treatment Of Produced Water From Nova Scotia

Gregory P. Thiel[1], Syed M. Zubair[2] and John H. Lienhard V[1]

[1] Department of Mechanical Engineering, Massachusetts Institute of Technology, Cambridge, MA, United States

[2] Department of Mechanical Engineering, King Fahd University of Petroleum and Minerals, Dhahran, Saudi Arabia

Address correspondence to Professor John H. Lienhard V, Massachusetts Institute of Technology, 77 Massachusetts Ave., Room 3-166, Cambridge MA 02139-4307, United States. Email: lienhard@mit.edu. Phone Number: +1 (617) 253-3790.

ABSTRACT

A significant barrier to further use of hydraulic fracturing to recover shale oil and/or gas is the treatment and/or disposal of hypersaline produced water. This work is an analysis of produced water from Nova Scotia, with the aim of understanding how scale impacts the choice of desalination system used in its treatment. Four water samples are presented, and for a representative case, the supersaturation of some likely scalants is estimated as a function of temperature, recovery ratio, and pH. This supersaturation map is then compared to conditions representative of common desalination systems, allowing the identification of limitations imposed by the water's composition. In contrast to many natural waters, it is found that sodium chloride is the most likely first solid to form at high recovery ratios, and that the top temperature of thermal desalination systems is unlikely to be scale-limited in the treatment of these waters.

INTRODUCTION

The use of hydraulic fracturing as a technique to recover vast amounts of new oil and natural gas is growing rapidly in North America and around the world [1,2]. Oil and gas obtained by hydraulic fracturing is bound in tight shale formations as little as about 30 meters in height located about 1200 to 3600 meters below the surface [3]. In order to recover this resource, a vertical well is drilled to the depth of the shale layer. The drill then turns and proceeds horizontally, i.e., parallel to the surface. A mixture of water, sand, and chemicals [3,4] is then pumped down the well causing small (micro) fissures to form in the shale layer, releasing the oil and/or gas contained within the formation. The sand, known as a proppant, keeps these fissures propped open, allowing the desired product to continue to escape from the shale after much of the fracturing fluid has returned to the surface.

Immediately following the fracture, an amount of fluid returns to the surface at relatively large flow rates. This is known as flowback, and consists mainly of the fracturing fluid itself. It is thus relatively low in total dissolved solids (TDS). The flowback continues for about 6–21 days [5]. About 30–40% of the initial quantity of fracturing fluid will return to the surface as flowback; because of its relatively low salinity, much of this can be reused without significant treatment in subsequent fracturing operations [6].

As time proceeds, a far more saline water returns to the surface at a much lower flowrate than the flowback. This water is known as produced water, because it is associated with a producing oil and/or gas well. The particularly high TDS of these waters—anywhere from 50 to 300 g/kg [3], or about 1.5 to nearly 9 times that of seawater—makes them unusable in subsequent fractures and well above salinities for safe disposal to natural aquifers.

Current industrial practice comprises three methods for handling these waters: (1) they may be trucked away for treatment; (2) they may be re-injected into the ground into disposal wells; or (3) they are treated *in situ*, using portable or centrally located treatment facilities.

All of these options pose challenges. In the case of trucking water away, the cost is generally high—typically 4 USD/bbl, or 34 USD/m^3 in the Marcellus for the transportation alone [7]—and most municipal treatment systems are not designed to handle high-TDS waters. The re-injection of wastewater into disposal wells has been linked with significant local seismicity, both in the U.S. states of Ohio [8] and Oklahoma [9]. Increasingly common is the third option, on-site desalination. As it both significantly reduces the volume of highly saline wastewater and allows a large portion of the wastewater to be reused in later fractures, this option is both environmentally and economically attractive.

However, because of the highly saline nature of produced water and the desire for high recovery ratios (the ratio of fresh water to feed water), treatment using conventional desalination systems poses a high risk of crystallization fouling, or scaling [10,11]. Unlike seawater and natural surface and ground waters, the scaling envelope for these produced waters is relatively unknown, meaning system performance, which is often scale-limited, leaves the user potentially under-informed during the technology selection process. Complicating the process further, produced water is highly diverse in both constituent ion species and TDS, making a generalized quantification of produced water scaling potential a gross oversimplification.

In this paper, an initial attempt to close this gap is made through consideration of the scaling potential of particular produced waters. Data obtained from several produced water samples from wells located in Nova Scotia, Canada is presented and analyzed in order to identify the most likely scale-forming compounds. A list of possible scales is compiled, and their solubility is quantified using the saturation index, calculated at thermophysical conditions representative of common desalination systems. The Pitzer model [12,13] for mixed electrolytes, extended by Harvie and Weare [14] and Harvie et al. [15], which has been validated for the computation of highly saline natural waters, is used to calculate activity

coefficients. Finally, some brief insights on the effect of scale formation in desalination system selection for this produced water sample are presented.

PRODUCED WATER SAMPLE DATA

Four water samples of produced water from the Maritimes Basin in Nova Scotia, Canada were tested. The tests were performed by Microbac Laboratories, Inc. Each sample was tested for 27 possible dissolved ions: aluminum, arsenic, barium, beryllium, bicarbonate, boron, bromide, cadmium, calcium, chloride, chromium, cobalt, copper, iron, lead, lithium, magnesium, manganese, mercury, molybdenum, nickel, potassium, selenium, silver, sodium, strontium, and sulfate. Concentrations are not given where the result is lower than the resolution of the test.

[Table 1 about here]

The results of the test are shown in Table 1; the total concentration of the samples varies greatly, ranging from about 53 g/L to about 97 g/L, or roughly two to three times that of seawater. Individual ion counts are also highly diverse: boron is present at about 0.6 g/L in one sample but almost completely absent in all of the others. It should be noted that these samples do not perfectly (within 5–20%) satisfy electroneutrality, likely due to inaccuracies in chloride tests. Previous studies have also noted this discrepancy, and they adjusted the chloride count as appropriate [5].

Regrettably, complete pH and ion speciation data for the samples are unavailable. As a result, some assumptions are required in order to estimate the values of ionic strength shown in Table 1. Elsewhere in the literature [5], neutral to slightly acidic values of pH have been observed in produced water samples. The values of ionic strength shown in Table 1 were calculated under the following assumptions: all boron is present as $B(OH)_3$ (typical of natural

waters at neutral pH [16]); all carbon is bicarbonate, as this was the ion tested; copper, manganese, and magnesium are all divalent free ions.

METHOD OF SCALING ANALYSIS

In order for scale to form, the concentration of a dissolved compound must exceed its solubility limit, or become supersaturated. Supersaturation is quantified in a variety of ways throughout the literature, often as a function of the supersaturated concentration and the solubility, expressed as an algebraic difference, a ratio, or a percent [17]:

$$\Delta c = c - c_{\text{sat}} \qquad S = \frac{c}{c_{\text{sat}}} \qquad \sigma = S - 1 \tag{1}$$

where c is the supersaturated concentration, and c_{sat} is the solubility. However, the solubility may vary significantly with temperature, pressure, pH, and the concentration and species of other dissolved compounds. Thermodynamically, crystallization is favored when a compound's activity product exceeds its solubility product. Thus, supersaturation is best quantified, particularly in mixed electrolyte systems, by the saturation index:

$$\text{SI} = \log\left(\frac{Q}{K_{sp}}\right) \tag{2}$$

where Q is the ionic activity product, and K_{sp} is the solubility product, both defined in the usual way [18,19].

Because the calculation of the saturation index involves the computation of an individual ion's activity, it is, in general, a non-trivial task. This is particularly so for mixtures of high ionic strength, where Debye-Hückel theory [20] is not applicable. The general procedure for calculating SI from water sample data is iterative, and is outlined as follows. First, individual ions are compared to a database containing possible scales (solid, soluble compounds composed of those ions) and available thermodynamic data. Values of the solubility product for each scale are then computed and corrected to the desired temperature. Activity

coefficients are calculated using Pitzer's model, and the speciation of ions at the given temperature and pH is computed iteratively. Finally, the saturation index is calculated according to Eq. (2). The details of each of these steps follow. All equations are implemented in MATLAB.

Calculation of the Solubility Product

The solubility product is defined as

$$K_{sp} = \exp(-\Delta_r G/RT) = a_M^{\nu_M} a_X^{\nu_X} a_W^{\nu_W} \tag{3}$$

where $\Delta_r G$ is the standard Gibbs free energy change of reaction, a is activity, and ν is the stoichiometric coefficient. The subscripts M, X, and W indicate cation, anion, and water (for a hydrated compound), respectively. Values of the solubility product are corrected from their reference temperature to the desired temperature using van 't Hoff's law, integrated assuming a constant $\Delta_r C_P$, when the data are available (for a derivation, see, e.g., [18]):

$$\ln\left(\frac{K}{K^\circ}\right) = \frac{\Delta_r H^\circ}{R}\left(\frac{1}{T^\circ} - \frac{1}{T}\right) + \frac{\Delta_r C_P^\circ}{R}\left[\ln\left(\frac{T}{T^\circ}\right) - 1 + \left(\frac{T^\circ}{T}\right)\right] \tag{4}$$

Values of $\Delta_r G$ and K_{sp} are taken from [21,22].

Calculation of Activity Coefficients

The calculation of a single ion's activity coefficient is performed using the semi-empirical Pitzer model [12,13], extended by Harvie and Weare [14] and Harvie et al. [15]. An excellent review of the Pitzer model and other models for calculating activity coefficients can be found in Zemaitis et al. [18]. It is derived from a virial expansion of the excess Gibbs free energy, and captures the effects of cation-cation, cation-anion, anion-anion, cation-cation-anion, and anion-anion-cation interaction. The model has been validated for solutions of high ionic strength (see, e.g., Zemaitis et al. [18] and Pabalan and Pitzer [23]). It should be noted that the activity coefficient of a single ion has no true physical meaning, as the condition of electroneutrality requires the presence of an ion of opposite charge to be present in a real-world system. The model summary given here roughly follows Harvie et al. [15]. For an

electrolyte MX that dissociates into cation M and anion X, the molal ionic activity coefficients are given by:

$$\ln \gamma_M = z_M^2 F + \sum_a m_a(2B_{Ma} + ZC_{Ma}) + \sum_c m_c(2\Phi_{Mc} + \sum_a m_a \Psi_{Mca})$$

$$+ \sum \sum_{a<a'} m_a m_{a'} \Psi_{aa'M} + |z_M| \sum_c \sum_a m_c m_a C_{ca} + \sum_n m_n(2\lambda_{nM}) \quad (5)$$

for the cation, and an analogous expression for the anion:

$$\ln \gamma_X = z_X^2 F + \sum_c m_c(2B_{cX} + ZC_{cX}) + \sum_a m_a(2\Phi_{Xa} + \sum_c m_c \Psi_{Xac})$$

$$+ \sum \sum_{c<c'} m_c m_{c'} \Psi_{cc'X} + |z_X| \sum_c \sum_a m_c m_a C_{ca} + \sum_n m_n(2\lambda_{nM}) \quad (6)$$

The osmotic coefficient is given by:

$$(\phi - 1) \sum_i m_i = 2[-A^\phi I^{3/2}/(1 + 1.2\sqrt{I}) + \sum_c \sum_a m_c m_a (B_{ca}^\phi + ZC_{ca})$$

$$+ \sum \sum_{c<c'} m_c m_{c'} \left(\Phi_{cc'}^\phi + \sum_a m_a \Psi_{cc'a}\right)$$

$$+ \sum \sum_{a<a'} m_a m_{a'} (\Phi_{aa'}^\phi + \sum_c m_c \Psi_{aa'c})$$

$$+ \sum_n \sum_a m_n m_a \lambda_{na} + \sum_n \sum_c m_n m_c \lambda_{nc}] \quad (7)$$

where z is the charge number, m is molality, λ is a parameter representing interactions between neutral and charged species, Ψ represents ternary interactions, $Z = \sum_i m_i |z_i|$, and the functions F, B, C, and Φ are defined below. The lowercase subscripts c, a, and n indicate summation over all cations, anions, and neutral species (e.g., aqueous carbon dioxide), respectively. The notation $a<a'$ and $c<c'$ indicate summation over all distinguishable pairs of anions and cations, respectively. The function F is

$$F = -A^\phi \left(\frac{\sqrt{I}}{1+1.2\sqrt{I}} + \frac{2}{1.2} \ln\left(1 + 1.2\sqrt{I}\right)\right) + \sum_c \sum_a m_c m_a B'_{ca}$$

$$+ \sum \sum_{c<c'} m_c m_{c'} \Phi'_{cc'} + \sum \sum_{a<a'} m_a m_{a'} \Phi'_{aa'} \quad (8)$$

where I is ionic strength, and A^ϕ is related to the Debye-Hückel parameter:

$$A^{\phi} = \frac{1}{3}\sqrt{\frac{2\pi N_A \rho_s}{1000}}\left(\frac{e^2}{\varepsilon k_B T}\right)^{3/2} \tag{9}$$

where N_A is Avogadro's number, ρ_s is the density of the solvent (water), e is the elementary charge, ε is the relative permittivity of the solvent, and k_B is Boltzmann's constant. The functions B, B', B^{ϕ}, and C represent interactions between unlike-charged pairs:

$$B_{MX} = \beta_{MX}^{(0)} + \beta_{MX}^{(1)}\, g\left(\alpha_{MX}\sqrt{I}\right) + \beta_{MX}^{(2)}\, g\left(12\sqrt{I}\right) \tag{10}$$

$$B'_{MX} = \beta_{MX}^{(1)}\, g'\left(\alpha_{MX}\sqrt{I}\right)/I + \beta_{MX}^{(2)}\, g'\left(12\sqrt{I}\right)/I \tag{11}$$

$$B_{MX}^{\phi} = \beta_{MX}^{(0)} + \beta_{MX}^{(1)} e^{-\alpha_{MX}\sqrt{I}} + \beta_{MX}^{(2)} e^{-12\sqrt{I}} \tag{12}$$

$$C_{MX} = \frac{C_{MX}^{\phi}}{2\,|z_M z_X|^{1/2}} \tag{13}$$

where $\alpha_{MX} = 2.0$ for n-1 electrolytes, $\alpha_{MX} = 1.4$ for 2-2 or higher electrolytes, and $\beta_{MX}^{(0)}$, $\beta_{MX}^{(1)}$, $\beta_{MX}^{(2)}$, and C_{MX}^{ϕ} are tabulated for a given ion pair. The parameter $\beta_{MX}^{(2)}$ is usually non-zero only for 2-2 electrolytes. The functions g and g' are defined as

$$g(x) = 2(1 - (1 + x)e^{-x})/x^2 \tag{14}$$

$$g'(x) = -\frac{2}{x^2}\left[1 - e^{-x}\left(1 + x + \frac{x^2}{2}\right)\right] \tag{15}$$

Interactions between like-charged pairs are represented by the functions Φ, Φ', and Φ^{ϕ}:

$$\Phi_{ij} = \theta_{ij} + {}^{E}\theta_{ij}(I) \tag{16}$$

$$\Phi'_{ij} = {}^{E}\theta'_{ij}(I) \tag{17}$$

$$\Phi_{ij}^{\phi} = \theta_{ij} + {}^{E}\theta_{ij}(I) + I\,{}^{E}\theta'_{ij}(I) \tag{18}$$

Here, the only adjustable parameter for a given ion pair is θ_{ij}. The terms ${}^{E}\theta_{ij}$ and ${}^{E}\theta'_{ij}$ represent excess free energy arising from electrostatic interactions between asymmetric ions (i.e., ions with charge of like sign and unlike magnitude), and are functions of ionic strength only.

In principle, each of the Pitzer parameters $\beta_{MX}^{(0)}$, $\beta_{MX}^{(1)}$, $\beta_{MX}^{(2)}$, C_{MX}^{ϕ}, λ, θ_{ij}, and Ψ are functions of temperature; however, that dependence is neglected in this analysis owing to incomplete data. A more recent, large collection of these parameters are available [24] as a function of temperature, but not all parameters are available over the temperature domain considered here. In addition, some derivatives of the Pitzer parameters with temperature at 25°C are available, e.g., from Pitzer [13]. However, these derivatives are often small [25], and it has been reported that much of the variation in activity coefficient with temperature is often confined to A^{ϕ}, both explicitly and implicitly through the strong temperature dependence of the relative permittivity [26]. In order to be internally consistent, the Pitzer parameters are taken as constants evaluated at 25°C, where the largest collection of data are available. As a result, the temperature dependence of the activity coefficients is confined to the Debye-Hückel parameter. Some estimates of the error induced by this approximation are given in the validation section below.

Particular values of the Pitzer parameters used in this work were taken from Harvie et al. [15] and Zemaitis et al. [18]. The range of molality (binary parameters) and ionic strength (ternary parameters) for which each parameter has been validated is given in Zemaitis et al. [18]. The extrapolation beyond these limitations, as can be the case at very high recovery ratios, may introduce some error. (See, e.g., Mistry et al. [27] for some discussion around the use of ionic strength to characterize mixed electrolyte behavior.)

Speciation Calculations

In order to account for ion pairs, the speciation of ion systems must be taken into account. In general, we wish to solve for the molalities of all forms of a particular species Y, such that equilibrium constants are satisfied, and mass and charge are conserved:

$$K = \frac{\prod_P (a^{\nu})_P}{\prod_R (a^{\nu})_R} \tag{19}$$

$$Y_T = \sum_i m_{Y,i} \quad (20)$$

$$\sum_i m_{Y,i} z_{Y,i} = 0 \quad (21)$$

where a is chemical activity, the subscript T indicates the total molality of species Y, and the subscripts P and R indicate multiplication over all products and reactants, respectively. Given a value of pH, these equations can be solved for the molalities $m_{Y,i}$.

Dissociation constants for particular ion pairs, such as $MgOH^+$ were selected according to the rules given by Harvie et al. [15], who found that experimental solubility data were accurately represented with and without the explicit inclusion of an ion pair only when the dissociation constant is above a threshold value. Below this threshold value, the tendency of the ions to associate is significant, and the ion pair must be explicitly included (i.e., its concentration and activity must be calculated in speciation computations).

VALIDATION

As mentioned above, the Pitzer model has been previously validated in the prediction of activity coefficients and mineral solubilities in mixed electrolytes. Nevertheless, a short validation of the present model follows in order to: (1) give a measure of confidence in the numerical implementation; and (2) estimate some of the error associated with the implementation of approximate temperature dependence, as discussed above. To do so, SI will be shown as a function of temperature, comparing the model described above to models with full temperature dependence in two example cases where full data on temperature dependence is available.

[Figure 1 about here.]

Figure 1 shows the saturation index as a function of temperature for NaCl at several concentrations. The open markers/dotted lines indicate the approximate temperature dependence, as implemented here, and the filled markers/solid lines indicate full temperature

dependence. To compute SI with full temperature dependence, both activity coefficients and solubility products as a complete function of temperature are required. The activity coefficients as a function of temperature are taken from tabulated data in Pitzer et al. [28]. Solubility products are calculated according to Eq. (3), where the Gibbs free energy as a function of temperature is computed using enthalpy and specific heat data from Pabalan and Pitzer [23]. As seen in Fig. 1, the difference in SI between the two models across the temperature domain here is less than 0.1.

Figure 2 shows the saturation index versus temperature for several $MgSO_4$ hydrates evaluated at experimental solubilities from Linke and Seidell [29]. A perfect prediction of the solubility would result in a calculated SI value of zero. In order to calculate the SI with full temperature dependence, again, both activity coefficients and solubility products are required as a function of temperature. The activity coefficients are computed using Eqs. (5) and (6) with temperature-dependent Pitzer parameters from Pabalan and Pitzer [23]. Solubility products are calculated according to Eq. (3), with Gibbs free energy as a function of temperature calculated from enthalpy and specific heat data given by Pabalan and Pitzer [23] and Archer and Rard [30]. Both models predict values of SI less than 0.05 for temperatures up to about 50°C, after which the present method is less satisfactory. Nevertheless, the difference in SI predicted by the full and approximate methods never exceeds about 0.3.

[Figure 2 about here.]

RESULTS AND DISCUSSION

Produced Water Test Case Sample

In the analysis that follows, a fictitious test-case sample was created that represents the data shown in Table 1. The composition of the fictitious, representative sample is given in Table 2. Note that, in contrast to the value shown in Table 1, the concentration of carbonates

is given as total carbonate, or total carbon (the sum of aqueous CO_2, HCO_3^-, H_2CO_3, and CO_3^{2-}), and not bicarbonate. Given in this manner, the value is pH independent. In order to satisfy electroneutrality, individual ion concentrations may deviate slightly from exact averages over the four data samples. Concentrations here are given in mg per kg solution; we have used a representative density of 1.04 kg/L in the conversion from mg/L. For reference, a sodium chloride solution with a TDS of 60 ppt has a density of 1.040 kg/L at 25°C; seawater has a density of 1.043 kg/L at the same TDS and temperature. Of course, because the sample is fictitious and only intended to represent real water samples, an exact value is not needed for this conversion. Note that borates are not considered in this test-case water, as they were only present in significant amounts in one of the four measured samples shown in Table 1. The ionic strength of the sample was calculated under the same speciation assumptions as outlined above for the values in Table 1.

[Table 2 about here.]

Identification of Possible Scales

In general, the identification of possible scales from a water sample of given composition may seem a fairly simple matter of combinatorics, where possible scales comprise all neutrally-charged combinations of cations and anions. However, care must be taken to identify which combinations do and do not exist; to identify possible hydrates and polymorphs, whose thermodynamic behavior may differ significantly; and to identify potential non-binary scales. Data on certain compounds may or may not be readily available.

To the authors' estimation, then, Fig. 3 shows a list of twenty reasonably common possible *binary* scales, ranked in order of smallest to greatest solubility product at 25°C. These solids were selected from compounds listed in [21,22] that can dissolve into any two ions listed in Table 2. Where present and data available, only the least soluble (in terms of smallest K_{sp} value) hydrate or polymorph is shown in the figure. Values of the solubility

product were calculated according to Eq. (3), or taken from tabulated data when Gibbs free energy data were not available [21,22].

[Figure 3 about here.]

Parametric Analysis

What follows are the results of an attempt to describe the scaling potential of the test-case produced water through the calculation of the saturation index at conditions representative of typical desalination systems. In particular, the effects of three variables are presented: recovery ratio, up to 90%; pH, from 3–8, and temperature, from 25°C up to 80°C, which is near or above the top temperature in many thermal desalination systems. Some multistage flash (MSF) systems for seawater desalination operate at higher top temperature and higher pH; however, this pH range is more typical of produced water, and temperatures above 80°C may introduce increasing amounts of error in the present model, as discussed in the Validation section above.

Effect of recovery ratio. Recovery ratio is defined as the quotient of the product (fresh) water flow rate and the feed (incoming produced water) flow rate. Owing to a variety of concerns ranging from high salinity brine disposal to insufficient membrane strength, in typical seawater desalination systems, the recovery ratio rarely exceeds about 50%. However, because the cost of produced water disposal is a strong function of wastewater volume, high recovery ratios are desirable.

Figure 4 shows the saturation index of the carbonate scales with SI > -5 at pH = 6 and 25°C as a function of recovery ratio up to 90%; Figure 5 shows the chloride salts at the same conditions. With the exception of $Mg(OH)_2$, most scales with OH anions remain below a saturation index of 5 over the entire range of recovery ratio, and are thus not shown. ($Mg(OH)_2$ only barely exceeds SI = −5 at RR = 90%, pH = 6, and T = 25°C.) Despite carbonate salts being, in general, sparingly soluble—four of the five least soluble scales in

this system are carbonates (see Fig. 3)—calcium carbonate becomes supersaturated only once a recovery ratio of about 85% is reached at 25°C. Most other carbonate salts are able to remain in solution up to recovery ratios of 90% at this temperature and pH, though $SrCO_3$ is close to its saturation limit at that condition. Moreover, in contrast to typical seawater systems, an examination of Figure 5 shows that NaCl is the solid that places the limit on recovery ratio in this system at just over 80%.

[Figure 4 about here.]

[Figure 5 about here.]

Effect of pH. The effect of pH on the saturation index is an implicit result from ion speciation calculations. Scale-forming cations or anions that form aqueous complexes with H^+ or OH^- ions reduce the concentration of the scalant, thus lowering its ionic activity product and pushing the equilibrium away from saturation.

Figure 6 shows the saturation index of carbonate salts with SI > −5 as a function of pH, showing the expected efficacy of pH adjustment as a measure of scale control. Although the pH data on the samples presented here is incomplete, other samples in literature have values of pH ranging from about 5.5 to about 7. Thus, even a small adjustment in pH, e.g., from 6 to 5, will reduce the saturation index of all carbonate salts to −3 or below, allowing very high recovery ratios to be reached, effectively shifting the curve shown in Figure 4 to the right.

The inconsistency among the trends of SI between the various carbonate salts in Figure 6 is readily explained with a comparison to Figure 7, which shows the concentration of pH-dependent ions. As pH reaches about 6, most of the carbonate ions are present as bicarbonate, resulting in a flat curve for the $NaHCO_3$ saturation index in Figure 6. The concentration of free carbonate increases over the entire range of pH, ultimately dominating other forms of carbonate outside the range of interest.

[Figure 6 about here.]

[Figure 7 about here.]

A scale of particular concern in seawater desalination is $Mg(OH)_2$ (see, e.g., [31]), which can form at high pH. As shown in Figure 8, $Mg(OH)_2$ appears to remain subsaturated over the more acidic range of pH considered here. Moreover, the mass fraction of Mg^{2+} ions in seawater is an order of magnitude higher than the produced water test case shown in Table 2. This combination of slightly more acidic pH and lower Mg^{2+} concentration is likely to result in a lower risk for $Mg(OH)_2$ scaling relative to seawater systems. Nevertheless, if increases in pH occur outside the domain explored here (which can occur locally in multi-effect distillers [32]), particularly when coupled with high recovery ratios, $Mg(OH)_2$ scale may still form.

[Figure 8 about here.]

The reader is reminded that in varying pH in this analysis, the mass of total carbonate has been conserved. The release of CO_2, for example, which can occur in thermal desalination systems (see, e.g., Al-Rawajfeh et al. [33]), can increase the pH and would change the total carbonate concentration, resulting in a shift of these equilibrium curves. This analysis only considers equilibria where mass is conserved and the pressure is atmospheric.

Effect of temperature. The effect of temperature on solubility is well known to be problematic in water treatment, particularly in the case of inverse solubility compounds, or compounds that display a decreasing solubility with increasing temperature. Here, however, many of the compounds associated with inverse solubility—particularly those with a sulfate anion—are absent.

The result is shown in Figure 9, a plot of saturation index versus temperature for carbonate salts with $SI > -5$ at pH = 6 and RR = 0. Both $CaCO_3$ and $MgHCO_3$ display measures of inverse solubility (i.e., decreasing solubility with increasing temperature, or increasing SI with increasing temperature) over the range of temperatures presented, but both remain well below saturation (SI = 0) at RR = 0. At a recovery ratios of about 80%, the SI of

$CaCO_3$ increases by about 1 or so (see Fig 4.), indicating that the combination of high temperature and recovery ratio may cause saturation to be reached. However, with a slight decrease in pH, the use of an anti-scalant [34], or nanofiltration pretreatment [35], for example, the risk of $CaCO_3$ scaling can be reduced.

Although aragonite is generally the polymorph of calcium carbonate that scales in seawater thermal desalination systems, it is only kinetically preferred (see, e.g., Berner [36]), and is metastable under the conditions presented here. As a result, calcite is has an SI closer to zero in Fig. 9. This trend is consistent with the results of Plummer and Busenburg [37], who treat the temperature dependence of the solubility product in more detail. The solubility product for aragonite was calculated using data from Anderson and Crerar [38].

It should be emphasized again that, owing to lack of data, the temperature dependence of both activity coefficients and equilibrium constants are not complete in this model. Nevertheless it appears that, in contrast to many other natural waters where sulfate scale becomes particularly problematic in thermal systems, temperature is unlikely to be as significant a limiting factor in these particular produced waters.

[Figure 9 about here.]

Consequences for Desalination System Selection

In the treatment of highly saline produced water, where high disposal costs and high water consumption costs drive the desire for high recovery ratio treatment systems, scaling can present a huge challenge, particularly where scale-limited performance is an unknown. In the test case presented here, one significant traditional design limit may not apply—scale-limited top temperature. With pH adjustment for carbonate scale control, sodium chloride becomes the first likely solid to form at high recovery ratios. As a result of the lack of sulfate ions, many of the inverse solubility salts that limit the top temperature of thermal systems are

not present here, allowing desalination at much higher temperatures[1]. Furthermore, owing to the normal solubility behavior of the limiting scale, sodium chloride, the NaCl curve shown in Figure 5 is shifted right at higher temperatures. Combined with the availability of a high temperature thermal source (the combustion of gas from the producing well), robust, high-temperature thermal desalination may prove to be an attractive option in the treatment of these produced waters.

Finally, as a result of increasing interest in small-scale desalination in the produced water segment, there have been attempts to adapt existing systems originally envisaged for low-cost, low-maintenance, community-level drinking water treatment to this purpose. Two promising technologies in this area are membrane distillation, or MD [41–46], and humidification-dehumidification, or HDH [47–52]. HDH, which uses air as a carrier gas to evaporate pure water from a saline stream, may become a particularly attractive option. Although the use of a carrier gas limits the recovery attainable in a single pass, a system that recirculates brine several times through the system can achieve very high recovery ratios when not scale-limited. In treating produced water like the sample presented here, where sodium chloride is the primary solid of concern, the potential for high recovery combined with portability, scalability, and robust components may make a system like HDH highly effective in produced water treatment.

CONCLUSIONS

In this paper, the potential for scaling in the treatment of produced water from the Maritimes Basin in Nova Scotia, Canada is estimated. The following results were obtained:

[1] Active research into mitigation technologies like surface modification (see, e.g., [39,40]) may, in the future, remove the top-temperature limit from waters that do include significant concentrations of sulfates by slowing or inhibiting the nucleation of scale on process surfaces.

1. Data on the composition of produced water from four samples was presented, resulting in the determination of a 60 ppt test case to be used in subsequent analyses of Nova Scotian produced water.
2. The limiting scale in the treatment of these waters was found to be sodium chloride, with crystallization possible at recovery ratios around 80% or higher.
3. With minor pH adjustment, alkaline scales such as $Mg(OH)_2$, $CaCO_3$, and $SrCO_3$ were found unlikely to limit desalination system recovery ratios.
4. Traditional limits on thermal desalination system top temperature were shown to be inapplicable in the treatment of these waters.

ACKNOWLEDGMENTS

The authors would like to thank the King Fahd University of Petroleum and Minerals for funding the research reported in this paper through the Center for Clean Water and Clean Energy at MIT and KFUPM under project number R4-CW-08. We would also like to acknowledge the helpful comments of an anonymous reviewer, whose feedback greatly improved the quality of the manuscript.

NOMENCLATURE

Roman Symbols

A^ϕ Debye-Hückel parameter, $kg^{1/2}/mol^{1/2}$

a Chemical activity, -

B Pitzer binary interaction parameter (also B^ϕ), kg/mol

B' Pitzer binary interaction parameter, kg^2/mol^2

C Pitzer third virial coefficient (also C^ϕ), kg^2/mol^2

C_P Specific heat capacity, kJ/mol-K

c Concentration, mol/L

e Elementary charge, C

F Pitzer equation, defined by Eq. (8), -

G Gibbs free energy, kJ/mol

g, g' Pitzer function, defined by Eqs. (14) and (15)

H Enthalpy, kJ/mol

I Ionic strength, $\frac{1}{2}\sum_i m_i z_i^2$, mol/kg

K Equilibrium constant, -

K_{sp} Solubility product, -

k_B Boltzmann's constant, kJ/K

m Molality, mol/kg

N_A Avogadro's number, mol^{-1}

Q Ionic activity product, -

R Universal gas constant, kJ/mol-K

S Supersaturation ratio, -

SI Saturation index, -

T Temperature, °C or K

TDS Total dissolved solids, mg/L or mg/kg

Z Pitzer equation, $Z = \sum_i m_i|z_i|$, mol/kg

z Charge number, -

Greek Symbols

α Pitzer parameter, $kg^{1/2}/mol^{1/2}$

β Pitzer parameter (unlike-charged interactions), kg/mol

γ Molal activity coefficient, -

Δ_r Change of reaction

ε Relative permittivity, -

θ Pitzer parameter (like-charged interactions), kg/mol

${}^{E}\theta$ Pitzer parameter (like-charged interactions), kg/mol

${}^{E}\theta'$ Pitzer parameter (like-charged interactions), kg^2/mol^2

λ Pitzer parameter for neutral species, kg/mol

v Stoichiometric coefficient, -

ρ Density, kg/L

σ Supersaturation, $S - 1$, -

ϕ Osmotic coefficient, -

Φ Pitzer parameter (like-charged interactions; also Φ^{ϕ}), kg/mol

Φ' Pitzer parameter (like-charged interactions), kg^2/mol^2

Ψ Pitzer parameter (ternary interactions), kg^2/mol^2

Subscripts

M, *c* Cation

n Neutral species

P Products

R Reactants

s Solvent (water)

sat Saturation

X, *a* Anion

W Water

Superscripts

- Reference state

REFERENCES

[1] U. S. Energy Information Administration, *Annual Energy Outlook 2012*, Jun. 2012.

[2] International Energy Agency, *Golden Rules for a Golden Age of Gas*, 2012.

[3] U. S. Department of Energy and the National Energy Technology Laboratory, *Modern Shale Gas Development in the United States: A Primer*, 2009.

[4] Holditch, S. A., Getting the Gas out of the Ground, *Chemical Engineering Progress*, vol. 108, no. 8, pp. 41–48, 2012.

[5] Research Partnership to Secure Energy for America, *Produced Water Pretreatment for Water Recovery and Salt Production*, tech rep no. 08122-36, 2012.

[6] Bomgardner, M., Treating Water from Hydraulic Fracturing, *Chemical & Engineering News*, vol. 90, no. 42, pp. 13–16, 2012.

[7] Rassenfoss, S., From Flowback to Fracturing: Water Recycling Grows in the Marcellus Shale, *Journal of Petroleum Technology*, vol. 63, no. 7, pp. 48–51, 2011.

[8] Ohio Department of Natural Resources, *Preliminary Report on the Northstar 1 Class II Injection Well and the Seismic Events in the Youngstown, Ohio Area*, 2012.

[9] Keranen, K. M., Savage, H. M., Abers, G. A., and Cochran, E. S., Potentially Induced Earthquakes in Oklahoma, USA: Links between Wastewater Injection and the 2011 M_w 5.7 Earthquake Sequence, *Geology*, vol. 41, no. 6, pp. 699–702, 2013.

[10] Epstein, N., Thinking about Heat Transfer Fouling: A 5 × 5 Matrix, *Heat Transfer Engineering,* vol. 4, no. 1, pp. 43–56, 1983.

[11] Müller-Steinhagen, H., Heat Transfer Fouling: 50 Years After the Kern and Seaton Model, *Heat Transfer Engineering,* vol. 32, no. 1, pp. 1–13, 2011.

[12] Pitzer, K. S. and Kim, J. J., Thermodynamics of Electrolytes. IV. Activity and Osmotic Coefficients for Mixed Electrolytes, *Journal of the American Chemical Society*, vol. 96, no. 18, pp. 5701–5707, 1974.

[13] Pitzer, K. S., A Thermodynamic Model for Aqueous Solutions of Liquid-Like Density, *Reviews in Mineralogy and Geochemistry*, vol. 17, pp. 97–142, 1987.

[14] Harvie, C. E. and Weare, J. H., The Prediction of Mineral Solubilities in Natural Waters: the Na-K-Mg-Ca-Cl-SO_4-H_2O System from Zero to High Concentrations at 25°C, *Geochimica et Cosmochimica Acta*, vol. 44, pp. 981–997, 1980.

[15] Harvie., C. E., Møller, N., and Weare, J. H., The Prediction of Mineral Solubilities in Natural Waters: The Na-K-Mg-SO_4-OH-HCO_3-CO_3-CO_2-H_2O System to High Ionic Strengths at 25°C, *Geochimica et Cosmochimica Acta*, vol. 48, pp. 723–751, 1984.

[16] Morel, F. and Hering, J., *Principles and Applications of Aquatic Chemistry*, Wiley, 1993.

[17] Mullin, J. W., *Crystallization*, 4th ed., Butterworth-Heinemann, 2001.

[18] Zemaitis, J. F., Clark, D. M., Rafal, M., and Scrivner, N. C., *Handbook of Aqueous Electrolyte Thermodynamics*, Wiley-AIChE, 1986.

[19] Robinson, R. A. and Stokes, R. H., *Electrolyte Solutions*, 2nd rev. ed., Dover, 2002.

[20] Debye, P. and E. Hückel, Zur Theorie der Elektrolyte, *Physikalische Zeitschrift*, vol. 24, no. 9, pp. 185–206, 1923.

[21] *Knovel Critical Tables*, 2nd ed., Knovel, 2008.

[22] *CRC Handbook of Chemistry and Physics*, 93rd ed., CRC Press, Boca Raton, 2012.

[23] Pabalan, R. T. and Pitzer, K. S., Thermodynamics of Concentrated Electrolyte Mixtures and the Prediction of Mineral Solubilities to High Temperatures for Mixtures in the system Na-K-Mg-Cl-SO_4-OH-H_2O, *Geochimica et Cosmochimica Acta*, vol. 51, pp. 2429–2443, 1987.

[24] Millero, F. and Pierrot, D., A Chemical Equilibrium Model for Natural Waters, *Aquatic Geochemistry*, vol. 4, pp. 153–159, 1998.

[25] Silvester, L. F. and Pitzer, K. S., Thermodynamics of Electrolytes. X. Enthalpy and the Effect of Temperature on the Activity Coefficients, *Journal of Solution Chemistry*, vol. 7, no. 5, pp. 327–337, 1978.

[26] Silvester, L. F. and Pitzer, K. S., Thermodynamics of Electrolytes. 8. High-Temperature Properties, Including Enthalpy and Heat Capacity, with Application to Sodium Chloride, *The Journal of Physical Chemistry*, vol. 81, no. 19, pp. 1822–1828, 1977.

[27] Mistry, K., Hunter, H. A., and Lienhard V, J. H., Effect of Composition and Nonideal Solution Behavior on Desalination Calculations for Mixed Electrolyte Solutions with Comparison to Seawater, *Desalination*, vol. 318, pp. 34–47, 2013.

[28] Pitzer, K. S., Peiper, J. C., and Busey, R. H., Thermodynamic Properties of Aqueous Sodium Chloride Solutions, *Journal of Physical and Chemical Reference Data*, vol. 13, no. 1, pp. 1–102, 1984.

[29] Linke, W. and Seidell, A., *Solubilities* Vol. II, 4th ed., American Chemical Society, 1965.

[30] Archer, D. G., and Rard, J. A., Isopiestic Investigation of the Osmotic and Activity Coefficients of Aqueous $MgSO_4$ and the Solubility of $MgSO_4 \cdot 7H_2O$(cr) at 298.15 K: Thermodynamic Properties of the $MgSO_4 + H_2O$ System to 440 K, *Journal of Chemical & Engineering Data*, vol. 43, pp. 791–806, 1998.

[31] Spiegler, K. S., and Laird, A. D. K., *Principles of Desalination*, 2nd ed., Academic Press, 1980.

[32] Glade, H., Krömer, K., Will, S., Loisel, K., Nied, S., Detering, J., and Kempter, A., Scale Formation and Mitigation of Mixed Salts in Horizontal Tube Falling Film Evaporators for Seawater Desalination, in Malayeri, M. R., Müller-Steinhagen, H., and Watkinson, A. P. (Eds.), *Proceedings of the 10th International Conference on Heat Exchanger Fouling and Cleaning*, Budapest, pp. 386–396, 2013.

[33] Al-Rawajfeh, A., Glade, H., and Ulrich, J., Scaling in Multiple-Effect Distillers: the Role of CO_2 Release, *Desalination*, vol. 182, pp. 205–219, 2005.

[34] Müller-Steinhagen, H., Malayeri, M. R., and Watkinson, A. P., Heat Exchanger Fouling: Mitigation and Cleaning Strategies, *Heat Transfer Engineering*, vol. 32, no. 3–4, pp. 189–196, 2011.

[35] Al-Rawajfeh, A. E., Fath, H. E. S., and Mabrouk, A. A., Integrated Salts Precipitation and Nano-Filtration as Pretreatment of Multistage Flash Desalination System, *Heat Transfer Engineering*, vol. 33, no. 3, pp. 272–279, 2012.

[36] Berner, R. A., The Role of Magnesium in the Crystal Growth of Calcite and Aragonite from Sea Water, *Geochimica et Cosmochimica Acta*, vol. 39, pp. 489–504, 1975.

[37] Plummer, L. N. and Busenberg, E., The Solubilities of Calcite, Aragonite and Vaterite in CO_2-H_2O Solutions between 0 and 90ºC, and an Evaluation of the Aqueous Model for the System $CaCO_3$-CO_2-H_2O, *Geochimica et Cosmochimica Acta*, vol. 46, pp. 1011–1040, 1982.

[38] Anderson, G. M., and Crerar, D. A., *Thermodynamics in Geochemistry: The Equilibrium Model*, Oxford University Press, 1993.

[39] Zettler, H. U., Wei, M., Zhao, Q., and Müller-Steinhagen, H., Influence of Surface Properties and Characteristics on Fouling in Plate Heat Exchangers, *Heat Transfer Engineering*, vol. 26, no. 2, pp. 3–17, 2005.

[40] Al-Janabi, A., Malayeri, M. R., and Müller-Steinhagen, H., Minimization of $CaSO_4$ Deposition Through Surface Modification, *Heat Transfer Engineering*, vol. 32, no. 3–4, pp. 291–299, 2011.

[41] Alkhudhiri, A., Darwish, N., and Hilal, N., Treatment of High Salinity Solutions: Application of Air Gap Membrane Distillation, *Desalination*, vol. 287, pp. 55–60, 2012.

[42] Saffarini, R., Summers, E. K., Arafat, H. A., and Lienhard V, J. H., Technical Evaluation of Stand-Alone Solar-Powered Membrane Distillation Systems, *Desalination*, vol. 286, pp. 332–341, 2012.

[43] Saffarini, R., Summers, E. K., Arafat, H. A., and Lienhard V, J. H., Economic Evaluation of Stand-Alone Solar-Powered Membrane Distillation Systems, *Desalination*, vol. 299, pp. 55–62, 2012.

[44] Summers, E. K., Arafat, H. A., and Lienhard V, J. H., Energy Efficiency Comparison of Single Stage Membrane Distillation (MD) Desalination Cycles in Different Configurations, *Desalination*, vol. 290, pp. 54–66, 2012.

[45] Summers, E. K. and Lienhard V, J. H., A Novel Solar Air-Gap Membrane Distillation System, *Desalination and Water Treatment*, vol. 51, pp. 1344–1351, 2013.

[46] Summers, E. K. and Lienhard V, J. H., Experimental Study of Thermal Performance in Air Gap Membrane Distillation Systems including Direct Solar Heating of Membranes, *Desalination*, vol. 330, pp. 100–111, 2013.

[47] Narayan, G. P., Sharqawy, M. H., Summers, E. K., Lienhard V, J. H., Zubair, S. M., and Antar, M. A., The Potential of Solar-Driven Humidification-Dehumidification Desalination for Small-Scale Decentralized Water Production, *Renewable and Sustainable Energy Reviews*, vol. 14, no. 4, pp. 1187–1201, 2010.

[48] Narayan, G. P., and Lienhard V, J. H., Thermal Design of Humidification Dehumidification Systems for Affordable Small-Scale Desalination, *IDA Journal*, vol. 4, no. 3, pp. 24–34, 2012.

[49] McGovern, R. K., Thiel, G. P., Narayan, G. P., Zubair, S. M., and Lienhard V, J. H., Performance Limits of Single and Dual Stage Humidification Dehumidification Desalination Systems, *Applied Energy*, vol. 102, pp. 1081–1090, 2013.

[50] Narayan, G. P., St. John, M. S., Zubair, S. M., and Lienhard V, J. H., Thermal Design of the Humidification Dehumidification Desalination System: An Experimental Investigation, *International Journal of Heat and Mass Transfer*, vol. 58, pp. 740–748, 2013.

[51] Sievers, M. A. and Lienhard V, J. H., Design of Flat-Plate Dehumidifiers for Humidification-Dehumidification (HDH) Desalination Systems, *Heat Transfer Engineering*, vol. 34, no. 7, pp. 543–561, 2013.

[52] Sievers, M.A. and Lienhard V, J. H., Design of Plate-Fin Tube Dehumidifiers for Humidification-Dehumidification Desalination Systems, *Heat Transfer Engineering*, accepted, Dec. 2013.

Table 1: Constituent ion data from the four produced water samples

Ion	Concentration (mg/L)			
	No. 1	**No. 2**	**No. 3**	**No. 4**
Aluminum			0.26	
Barium			0.85	6
Bicarbonate	68	124	58	
Boron	580		0.59	
Calcium		920	670	773
Chloride	37900	63700	38300	33000
Copper			0.072	
Magnesium	272	518	316	309
Manganese			0.52	
Potassium		200	83	37
Sodium	19000	32000	22000	19200
Strontium	20	8	7	8.7
TDS (mg/L)	57840	97470	62159	53334
I (mol/L)	0.98	1.69	1.08	0.95

Table 2. Composition of representative, test-case produced water from Nova Scotia

Ion	**Mass Fraction (mg/kg-soln)**	**Millimolal (mmol/kg-solv)**
Barium	1.6	0.0128
Calcium	568	15.1
Carbonate	83	1.41
Chloride	36221	1090
Magnesium	340	14.9
Potassium	77	2.10
Sodium	22164	1030
Strontium	11	0.128
Total	59465.6	2154
Ionic Strength	-	1093

List of Figure Captions

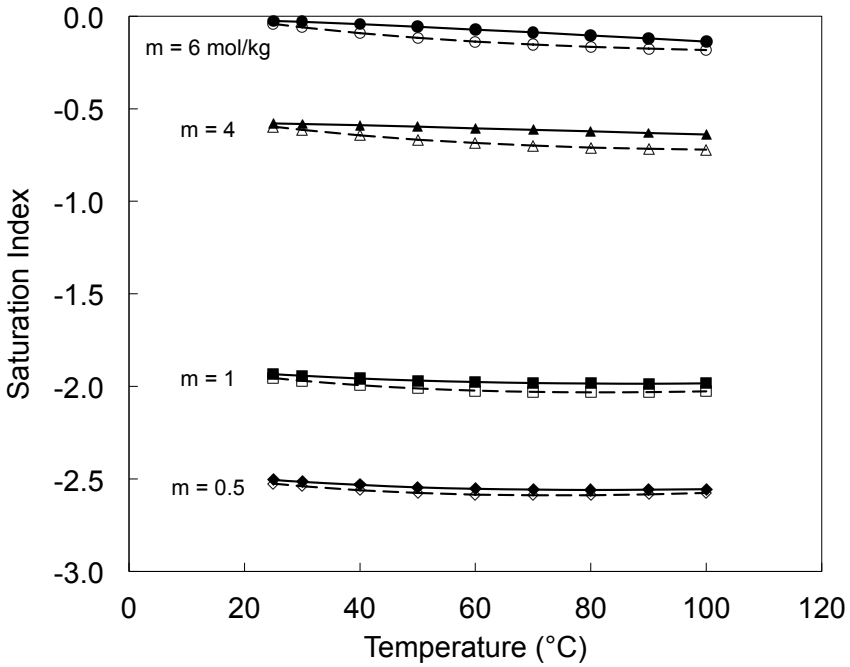

Figure 1. Saturation index versus temperature of NaCl at the indicated molalities. Solid lines correspond to full temperature dependence; dotted lines correspond to the approximate method in the present work.

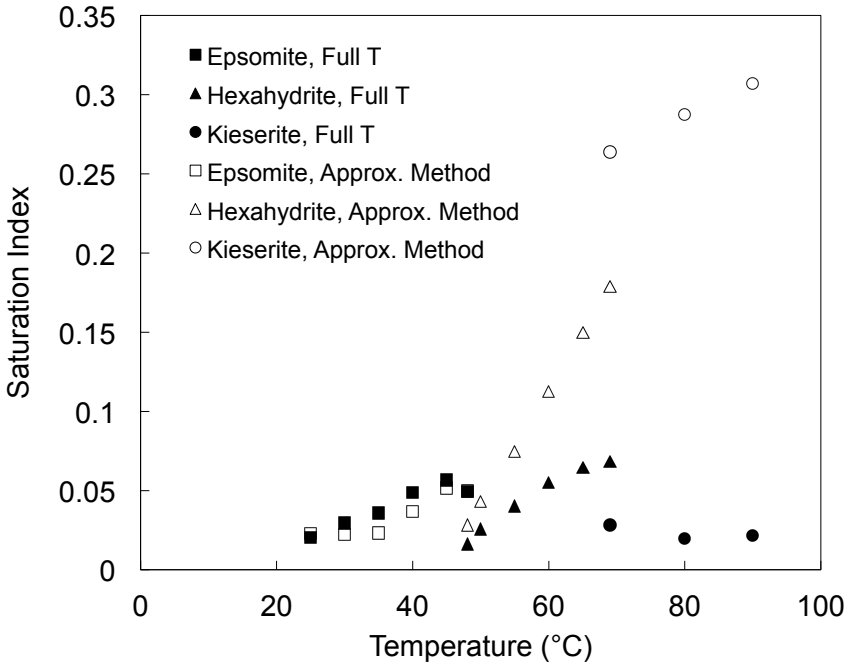

Figure 2. Values of saturation index versus temperature evaluated at experimental solubilities

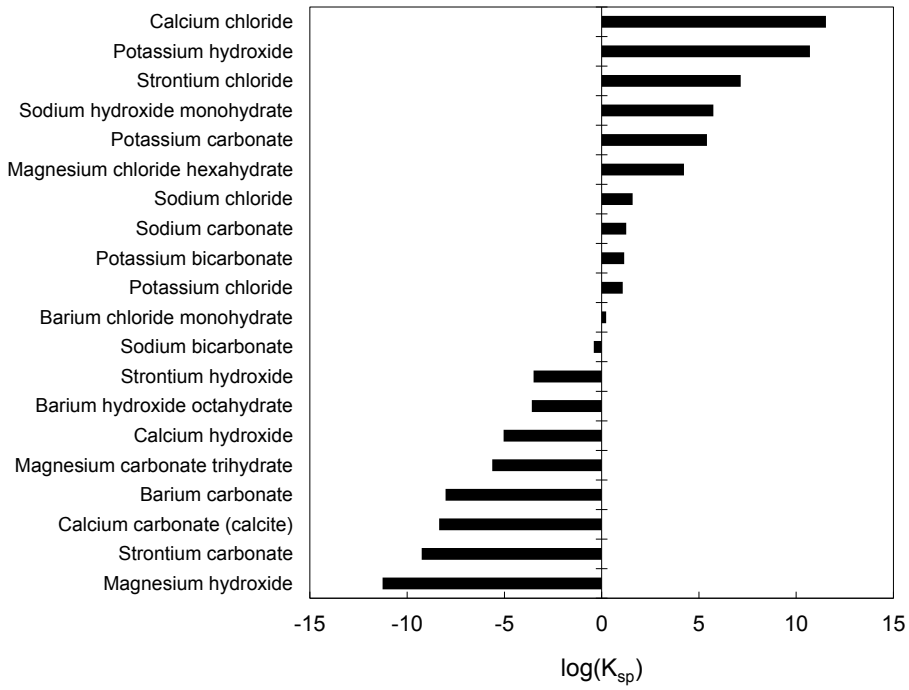

Figure 3. Possible scales from test-case Nova Scotia produced water

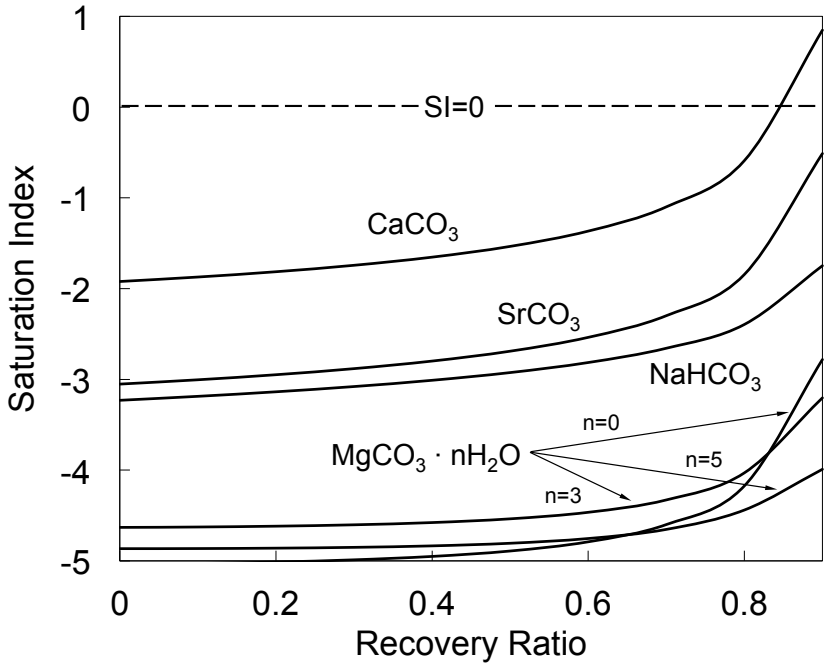

Figure 4: Saturation index vs. recovery ratio for carbonate salts with SI > -5 at pH = 6 and *T* = 25°C

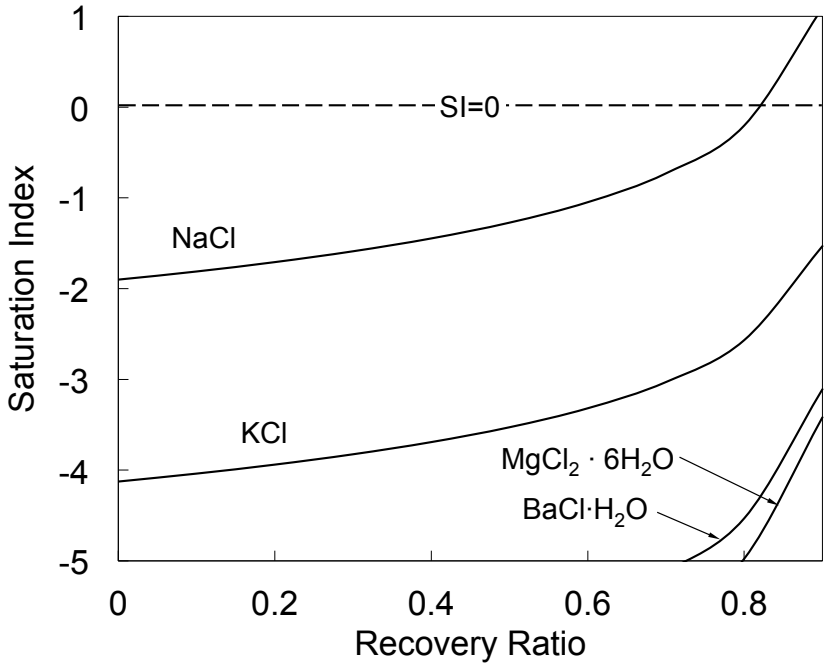

Figure 5: Saturation index vs. recovery ratio for chloride salts with SI > -5 at pH = 6 and T = 25°C

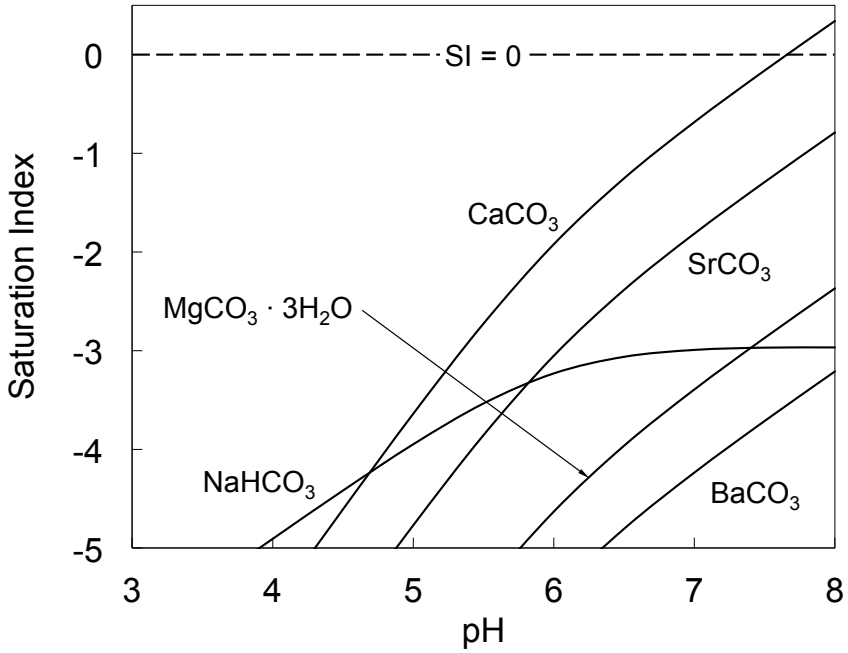

Figure 6: Saturation index vs. pH for carbonate salts with SI > -5 at RR = 0 and T = 25°C

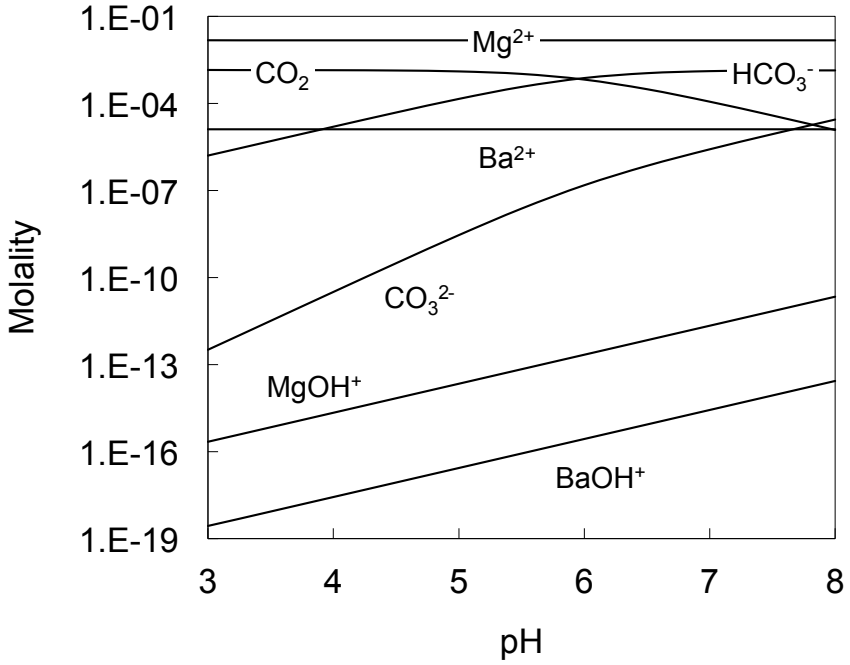

Figure 7: Concentration of pH-dependent ions in the test-case water sample.

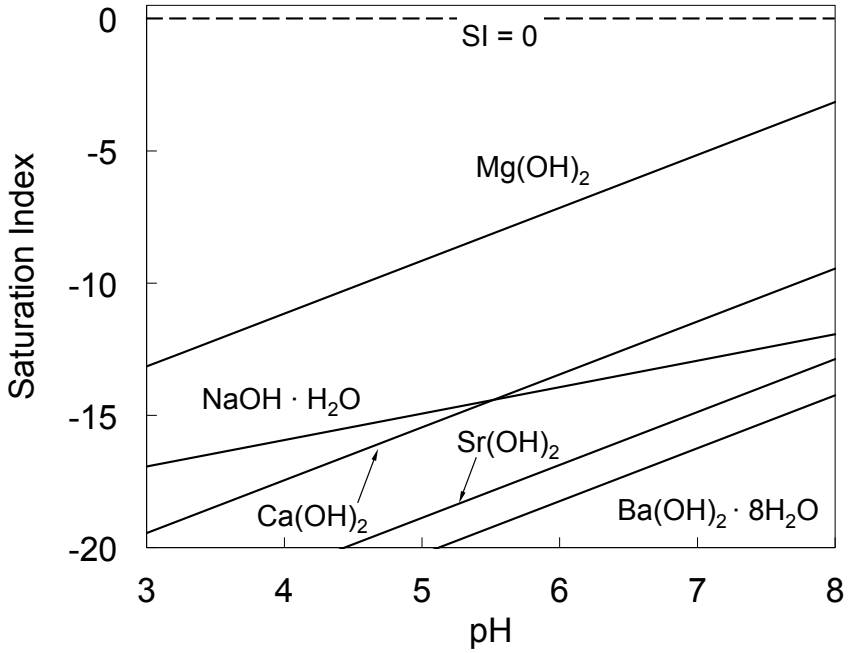

Figure 8: Saturation index vs. pH for several solid compounds containing OH^- anions.

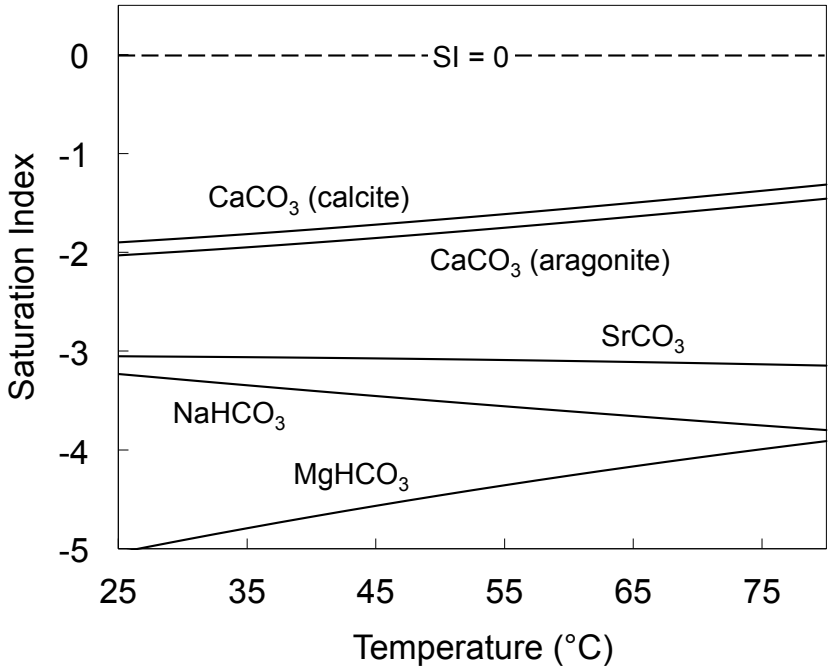

Figure 9: The variation of saturation index for carbonate scales with temperature at pH = 6, and RR = 0.

Gregory P. Thiel is a Ph.D. candidate in the Department of Mechanical Engineering at MIT. His research foci include hypersaline wastewater treatment, entropy generation minimization, and desalination system design. He is a recipient of the Martin Family Fellowship for Sustainability and an Eni-MIT Energy Initiative Fellowship. Greg holds an S.M. in mechanical engineering from MIT and a B.S.E. in mechanical engineering from Case Western Reserve University.

Dr. Syed M. Zubair is a Distinguished Professor in the Mechanical Engineering Department at King Fahd University of Petroleum & Minerals (KFUPM). He earned his Ph.D. degree from Georgia Institute of Technology, Atlanta, Georgia, U.S.A., in 1985. He is active in both teaching and research in the area of thermal sciences. During the past twenty-seven years, he has taught several courses related to heat transfer and thermodynamics at both the graduate and undergraduate levels. He has participated in several externally and internally funded research projects here at KFUPM, and has published over 150 research papers in internationally referred journals. Due to his various activities in teaching and research, he was awarded Distinguished Researcher award by the university in academic years 1993-1994, 1997-1998, and 2005-2006 as well as Distinguished Teacher award in academic years 1992-1993 and 2002-2003.

John H. Lienhard V is the Samuel C. Collins Professor of Mechanical Engineering at MIT. During more than 25 years on the MIT faculty, Lienhard's research and educational efforts have focused on heat transfer, desalination, thermodynamics, fluid mechanics, and instrumentation. He has also filled a number of administrative roles at MIT. Lienhard received his bachelors and masters degrees in thermal engineering at UCLA from the Chemical, Nuclear, and Thermal Engineering Department, and his PhD from the Applied Mechanics and Engineering Science Department at UC San Diego. He has been the Director of the Rohsenow Kendall Heat Transfer Laboratory since 1997, and he is the Director of the Center for Clean Water and Clean Energy at MIT and KFUPM.